Development of Polar Direct Drive Designs for Initial NIF Targets

Alexandra M. Cok

Allendale Columbia School

Rochester, New York

Advisor: Dr. R. S. Craxton

Laboratory for Laser Energetics

University of Rochester

Rochester, New York

November 2006

Abstract

This work proposes a means by which the National Ignition Facility (NIF) laser system, being built for indirect-drive laser fusion, can be used for symmetric direct-drive implosions producing high fusion neutron yields as soon as the NIF is operational. It uses polar direct drive (PDD), which involves repointing the laser beams away from the center of the target in an attempt to maintain shell radius uniformity during the implosion. All PDD designs proposed to date need specially designed phase plates that will not be available for initial NIF experiments. However, this work shows that good uniformity can still be obtained without special phase plates by certain combinations of defocusing and pointing of the beams, including pointing offsets of individual beams within the NIF laser beam quads, which are easy to implement. Two designs have been developed using the two-dimensional hydrodynamic simulation code SAGE. The first design uses the elliptical phase plates that will be used for indirect drive on the NIF; the second design uses no phase plates. Both designs will make high-yield direct-drive implosions possible with the initial NIF setup.

1. Introduction

Nuclear fusion provides a possible source of clean, abundant energy. One approach to fusion uses laser beams to irradiate a spherical target containing fuel comprised of deuterium and tritium, two isotopes of hydrogen, inside a shell of a material such as plastic or glass. The outside of the shell ablates outwards and the inside is compressed inwards, compressing the fuel to high densities and temperatures. The extreme temperature of the fuel overcomes the Coulomb repulsion forces of the positively charged nuclei, and the extreme compression ensures a large number of fusion reactions before the fuel explodes. The deuterium and tritium fuse to form a helium nucleus, releasing an energetic neutron. Most of the energy released by fusion reactions is

in the form of energetic neutrons. The energy of the helium nucleus is redeposited in the compressed fuel if the density and radius of the fuel are great enough. This redeposition of energy is known as ignition. Ignition is the first step to gaining breakeven, when the energy released from fusion reactions exceeds that input by the laser. Laser fusion will not be a viable source of abundant energy unless breakeven is achieved.

There are two different approaches to laser fusion: direct drive[1] and indirect drive[2]. With direct drive, laser beams hit the target pellet at normal incidence from all directions [Figure 1(a)]. This is the type of fusion for which the OMEGA laser system at the University of Rochester's Laboratory for Laser Energetics is configured. With indirect drive, the target pellet is surrounded by a "hohlraum", a cylinder made of gold or another material with a large atomic number [Figure 1(b)]. Laser beams enter the hohlraum through openings cut into the top and bottom. When hit by the laser beams, the hohlraum emits x rays, which then irradiate the target pellet, providing the energy needed for compression. Almost all of the initial laser energy is absorbed by the gold and close to 80% is reemitted as x rays. However, only 20% is actually absorbed by the target pellet; the rest is absorbed by the walls of the hohlraum or lost through the openings in the hohlraum. The lower energy efficiency of indirect drive is made up for by the greater uniformity of x ray radiation of the target. The National Ignition Facility (NIF), currently being constructed at Lawrence Livermore National Laboratory, will be configured for indirect drive.

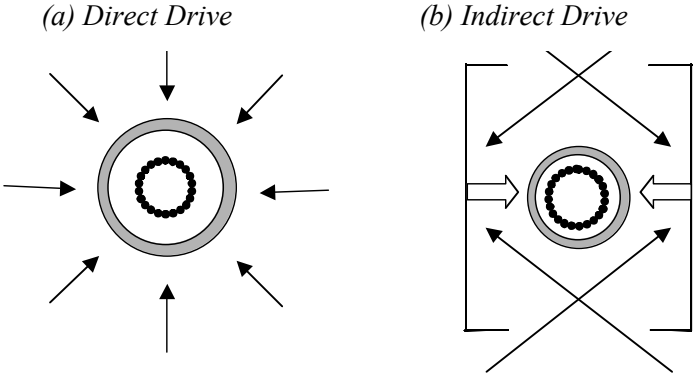

Figure 1. The two main approaches to laser fusion. (a) In direct drive, the laser beams irradiate the target pellet. Arrows represent laser beams and the dotted circle shows how the shell implodes. (b) In indirect drive, the target pellet is contained in a cylindrical hohlraum, which is hit by lasers entering through holes in the top and bottom of the hohlraum. The hohlraum produces x rays (open arrows), which irradiate the target.

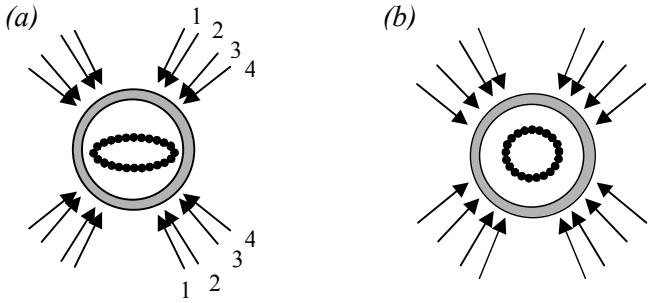

Figure 2. The possible ways in which the NIF laser beams, positioned for indirect drive, can irradiate a direct-drive target. (a) When the laser beams are aimed at the target center, the shell implodes nonuniformly. (b) Polar direct drive, in which the beams are repointed away from the center of the target, causes a nearly uniform implosion. Rings 1-4 are indicated in (a).

The NIF is due for completion in 2010, at which point it will become the world's most powerful laser. The NIF has 192 beams designed to deliver a total of 1.8 MJ of energy to the target, theoretically enough energy to achieve ignition and breakeven. The NIF laser beams are incident from the top and bottom of the target pellet. The laser beam ports are arranged in four rings at angles of 23.5°, 30.0°, 44.5°, and 50.0° from the vertical in the upper hemisphere with four corresponding rings in the lower hemisphere. There are a total of 48 ports; laser beams are arranged in groups of four called quads, so there is one quad per port. Each beam is square, measuring 40 cm by 40 cm. Symmetric direct-drive experiments, with a configuration similar to that shown in Figure 1(a), are not planned until around 2016, as this will involve repositioning half of the beams to another ring at 77.45°, an expensive and time-consuming process. A scheme termed polar direct drive (PDD)[3] has been proposed to enable earlier direct-drive experiments on the NIF. If the indirect-drive beams are simply aimed at the center of the target, as in Figure 2(a), the target shell receives significantly more drive on the poles than on the equator. As a result, the ratio of the shell velocity at the poles to the shell velocity at the equator is approximately two to one. Such distortion in the shell is not acceptable since shell radius uniformity is necessary to obtain high compression. The proposed PDD solution to this is to repoint the beams away from the center of the target, minimizing the differences in the amount of drive on all portions of the target shell [Figure 2(b)].

Prior to producing the energy required for ignition experiments (1.0 to 1.8 MJ), the NIF

laser system and diagnostic systems will be tested at an energy of 375 kJ to ensure that the laser optics are not damaged. In particular, the neutron diagnostic systems must be tested. Direct-drive fusion must be used to obtain the maximum number of neutrons at this energy, because at low energies indirect drive cannot provide sufficiently high temperatures and compression to yield as large a number of neutrons. Therefore, PDD designs maximizing the shell radius uniformity must be developed.

All previous PDD designs[3-6] required special phase plates (see Section 2.2 below). Unfortunately, these will not be available initially on the NIF. This work has investigated alternate ways of developing PDD designs, involving certain combinations of beam defocusing and pointing that are straightforward to implement. This work has resulted in two designs that will make the desired initial experiments possible.

2. Parameters Available for Optimization

The key parameters available for developing the two-dimensional designs are specifications for shifting the beam pointings away from the center of the target and defocusing the beams (Section 2.1). The optimum combinations of shifting and defocusing depend on the availability of indirect-drive phase plates (Section 2.2). Section 2.3 describes "split quads" in which the four beams are shifted slightly differently so that they do not overlap exactly.

2.1 Shifting and Defocusing

Figure 3(a) shows the important optics near the end of the laser system that control the parameters described here. The beam pointing is shifted away from the center of the target by moving the mirror. The center of the beam then moves a specified distance in the direction perpendicular to its axis, so that the beam hits the target at a different spot [Figure 3(b)].

Defocusing the beam is done by moving the focus lens toward the target. The laser beam

spot on the target is then enlarged and the maximum intensity decreases. To gain the best uniformity and overlap of laser beams, the diameter of the beam spot should generally correspond to the diameter of the target shell. Defocusing can be used to change the relative intensities of the four rings of beams as well as to change the size of each beam spot.

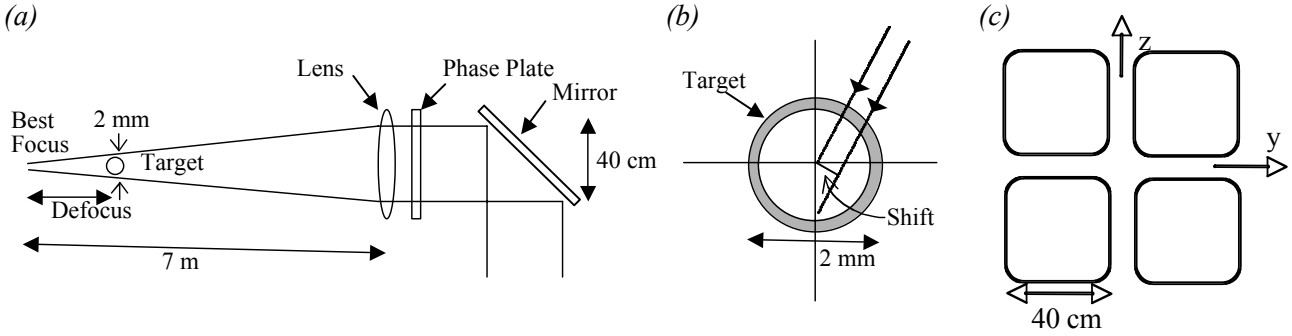

Figure 3. (a) Diagram (not to scale) showing the parts of the laser that control the parameters used in this work. Moving the lens along the beam axis controls the size of the beam at the target and tipping the mirror controls beam pointing. (b) Diagram showing how beam ring shifts are measured perpendicular to the beam direction. The angle of the beam from the vertical remains virtually constant. (c) Diagram showing the arrangement of four beams in a quad at the output of the laser system.

2.2 Phase Plates

Laser beams accumulate small irregularities in coherence after passing through the many amplification optics. These irregularities, if uncorrected, will imprint as hot spots on the target affecting the uniformity of the implosion. Phase plates[7,8] are special optics through which the beams pass before they are focused. A phase plate spreads the energy of the beam slightly to give a more uniform beam after focusing. Different types of phase plates are used to produce different sizes of beam spots. For direct drive, the beam spots need to be large to cover the target. For indirect drive, the beams need to be small enough to pass through the openings in the hohlraum without hitting the edges of the openings and generating plasmas (see Figure 4). Such plasmas would cause the laser beam rays to refract and strike the hohlraum wall in the wrong place or even prevent the rays from entering the hohlraum. The NIF will have two different types of phase plates: those for inner beams (rings one and two, see Figure 4) and those for outer beams

(rings three and four). The phase plates that will be used on the NIF will produce small elliptical focal spots because of the angles at which the beams enter the hohlraum (see Figure 4). The size of the spot depends on the angle at which the beams pass through the openings in the hohlraum. Therefore, since the beams in rings three and four enter at much shallower angles, their spot sizes must be smaller than those produced for rings one and two. The small spot sizes produced by the NIF indirect-drive phase plates make them unsuitable for direct-drive experiments unless the beams are defocused. The development of two PDD designs in this work, one with phase plates and one without, allows for flexibility depending on the availability of the NIF indirect-drive phase plates.

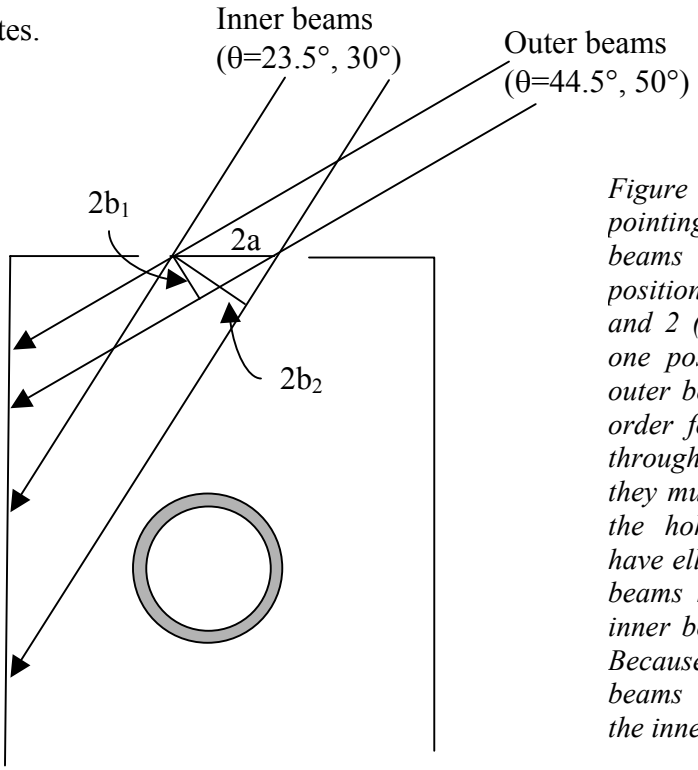

Figure 4. The proposed indirect drive pointings for the NIF. From each end, beams are aimed at two vertical positions on the hohlraum wall. Rings 1 and 2 (the inner beams) are aimed at one position and rings 3 and 4 (the outer beams) are aimed at another. In order for the beams to be able to fit through the openings in the hohlraum, they must be circular as they pass into the hohlraum. Therefore, the beams have elliptical cross sections. The outer beams have semi-axes (a, b_1) and the inner beams have semi-axes of (a, b_2). Because of the greater angle, the outer beams are much more elliptical than the inner beams.

Figure 5 shows a comparison of beams in best focus and beams out of focus, with and without phase plates. Figure 5(a) shows the intensity contours of a small ring-four best-focus spot without a phase plate, whose size is determined by the optical aberrations in the laser. Each contour represents a 10% increase in intensity, starting at 10% of peak intensity. Figure 5(b) shows a ring four beam in best focus with a phase plate. Figures 5(c) and (d) show the intensity

contours of a ring-four beam out of focus (defocused by 1.7 cm) with and without a phase plate. Without a phase plate, the best-focus spot is round. As the beam is taken farther out of best focus, the spot becomes increasingly square, corresponding to the square beam shape at the output of the laser.

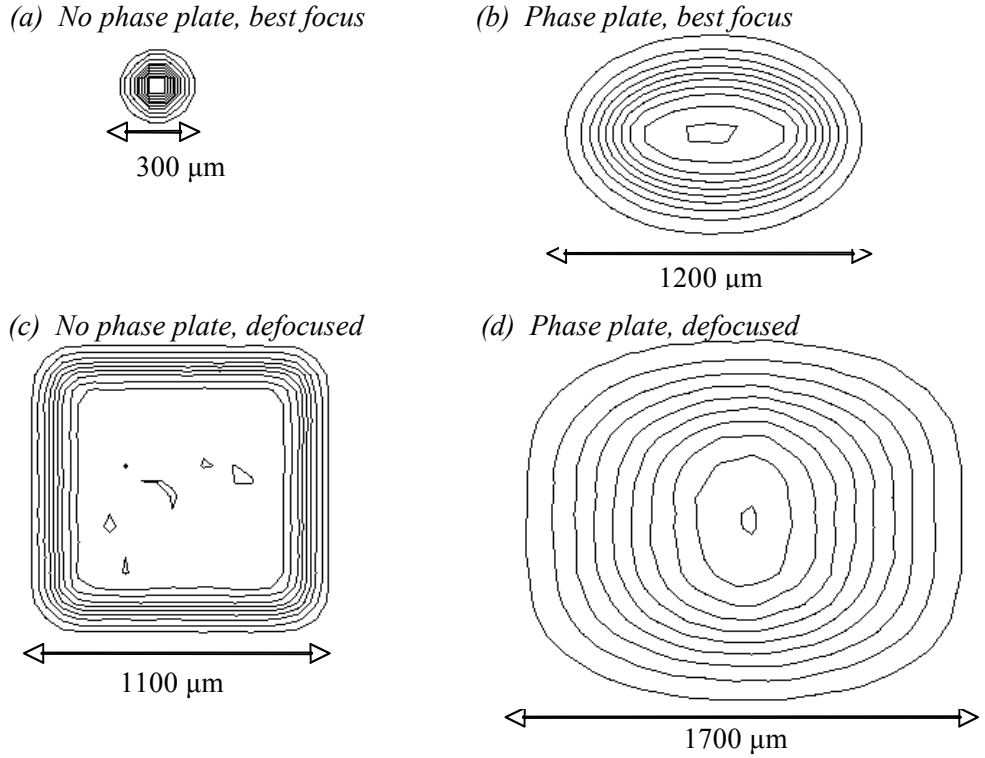

Figure 5. (a) The intensity contour plot of a ring 4 beam in best focus. (b) The intensity plot of a ring 4 beam with a phase plate in best focus. (c) A ring 4 beam without a phase plate, out of best focus with a defocus distance 1.7 cm. (d) A ring 4 beam with a phase plate, out of best focus with a defocus distance

2.3 Split Quads

The four beams of each quad, arranged at the output of the laser as shown in Figure 3(c), are usually focused down to a single focal spot. However, as each beam has an adjustable mirror, as shown in Figure 3(a), it is possible to adjust the pointings of the four beams so that they are focused to slightly different spots. This changes the overall shape of the intensity contours. Quads with pointings altered in this way will be referred to as "split quads." Using split quads, it is possible to alter the shape of the beams from the elliptical spots created by the phase plates and

to alter the rate at which the intensity of the beam drops off away from the center of the beam.

Intensity contour plots of ring four beams using split quads are shown in Figure 6. These beams are the same as those shown in Figure 5, except that in Figure 6 the beams have split quads. In Figures 6(a) and (b) each beam is in best focus with and without a phase plate. In Figure 6(c) and (d) each beam is out of focus (defocused by 1.7 cm). Figures 6(c) and (d) also show the actual ring-four beam profiles used in the designs described later in this report. The rate at which the intensity of the beam drops off away from the center of the beam is much less steep when using a split quad [compare Figures 5(c) and 5(d) to Figures 6(c) and 6(d)]. The difference is especially notable when not using a phase plate. By using a combination of split quad shifting and defocusing, the NIF beams can be enlarged by a factor of two or even more if necessary.

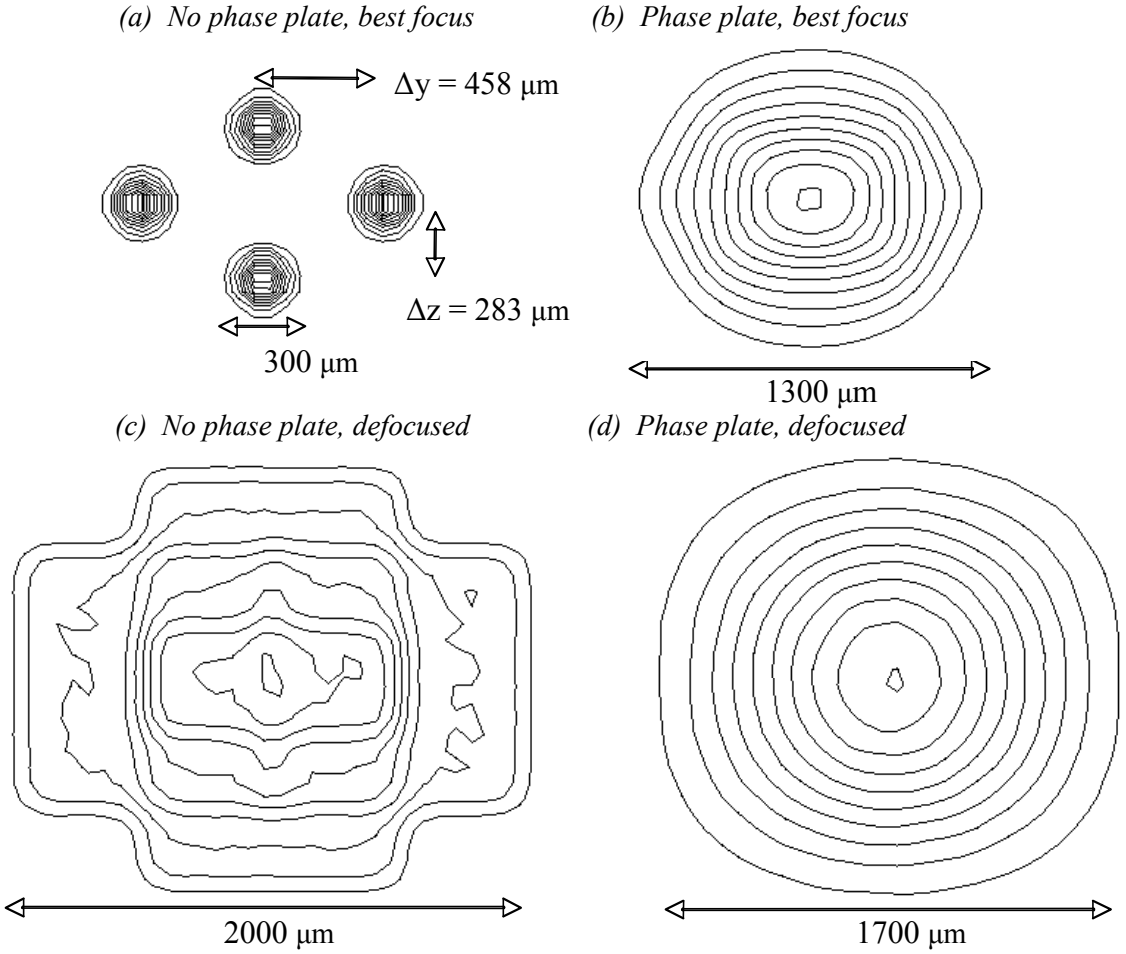

Figure 6. As in Figure 5, but each beam uses a split quad with shifts (Δz, Δy) = (283 μm, 458 μm) in (a) and (c) and (Δz, Δy) = (247 μm, 155 μm) in (b) and (d). (c) and (d) show the intensity contours of the ring 4 beams actually used in the designs discussed later in this report.

3. Target Design

The target designed to maximize the neutron yield at a total laser energy of 375 kJ is a shell of 8 μm of glass (SiO_2) with a radius of 1100 μm. The shell is filled with ten atmospheres of deuterium-tritium (DT) gas. The laser pulse used on this target is a Gaussian-shaped pulse shown in Figure 7(a). The pulse lasts a total of 5 ns with its peak power at 2.5 ns.[9]

When the laser pulse hits the target shell, the outer layers of the shell reach extreme temperatures and form a coronal plasma around the target. A plasma is a gaseous cloud of electrons and positively charged ions. The plasma expands outward and more layers are ablated as the laser power increases. The high pressure in the plasma causes the shell to accelerate inward. The motion of the center of mass of the shell, as predicted by the hydrodynamic code SAGE[10], is shown in Figure 7(b) as the red curve. Peak compression of the gas inside the target shell occurs just after 3 ns. Figure 7(b) also shows a number of density contours including the critical density (n_c), the density past which the laser cannot penetrate. Most of the laser energy is deposited between critical density and quarter-critical density ($n_c/4$).

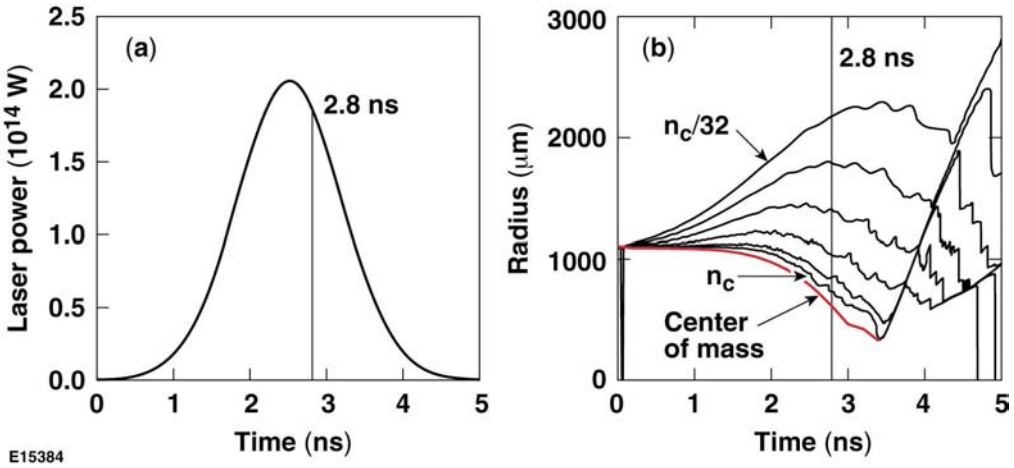

Figure 7. (a) Laser power versus time. This design used a Gaussian pulse. (b) Radius versus time of several density contours in the coronal plasma, including critical density (n_c). The outer layers of the shell ablate and expand outward, whereas the inner layers are compressed inwards. The center of mass of the imploding target shell is shown in red.

The implosion of the shell and the creation of a coronal plasma are shown in Figure 8. In Figure 8(a), a raytrace plot of the shell is shown near the start of the laser pulse when the shell is close to its starting position. The red lines represent the incoming rays from a ring-four laser beam. The black contours are density contours, and the green region shows the position of the shell. Figure 8(b) shows the shell at 2.8 ns, over halfway into the laser pulse. This plot shows the implosion of the optimum design with phase plates. The two plots provide a comparison between the starting shell and the shell when it has imploded halfway, and show that the shell has maintained its uniformity through 2.8 ns.

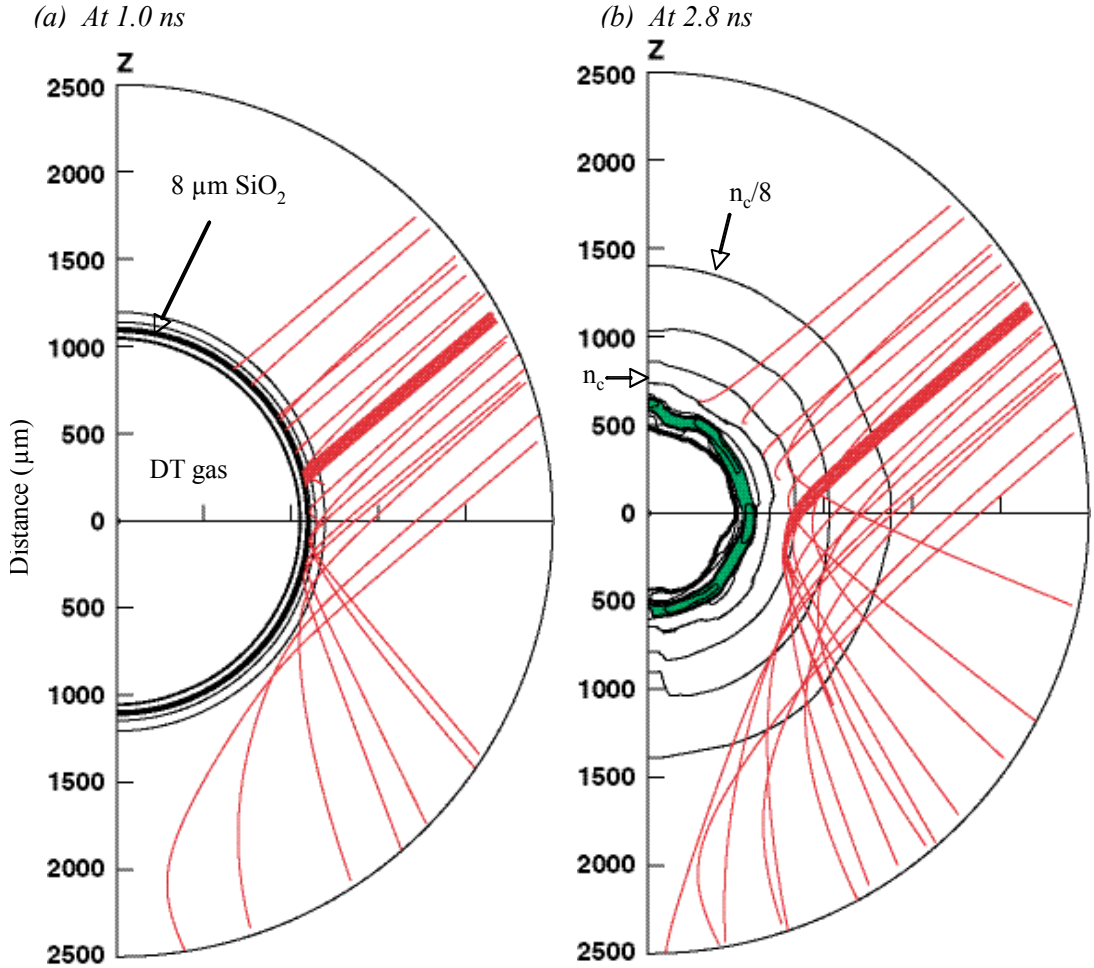

Figure 8. (a) A raytrace plot at 1.0 ns, near the start of the laser pulse. (b) A raytrace plot at 2.8 ns, when the shell (green) has imploded halfway. These plots show representative rays of ring 4 and some density contours. The design used for this simulation was the design with phase plates.

The importance of optimizing the designs is shown in Figure 9. In Figure 9(a), all of the beams are pointed to the center of the target and the defocus is 3.5 cm for all of the beams. The distortion in the shell at 2.8 ns is obvious as the shell forms an ellipse with semi-axes of 400 μm and 750 μm. The ratio of velocities between the poles and the equator is 1.7 to 1 at 2.8 ns. Figure 9(b) shows the optimum design without phase plates at the same time. Raytrace plots such as Figures 8 and 9 show where each ring of beams hits the target, how well the shell maintains uniformity as it implodes, and where distortions in the shell occur.

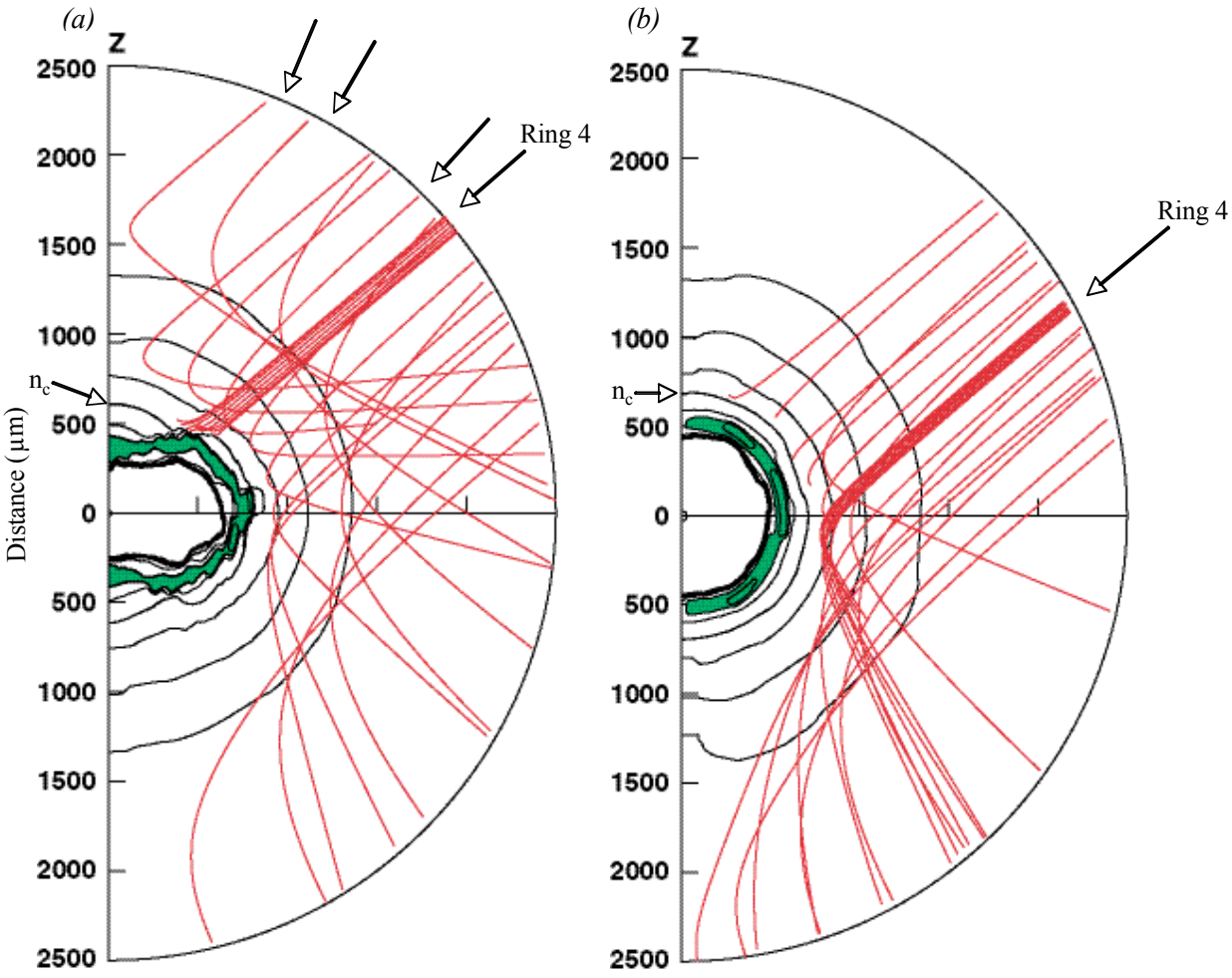

Figure 9. A comparison of two SAGE raytrace plots at 2.8 ns. (a) shows the implosion when the design has not been optimized, with all beams pointed to the center of the target. There is significant distortion in the shell. (b) shows the implosion when the design is highly optimized, and the shell maintains its uniformity. The optimized design used for (b) was the design without phase plates.

The two optimum designs, illustrated in Figures 8(b) and 9(b), were developed after numerous simulations using SAGE. SAGE provides parameters enabling the user to adjust the beam profiles. Although the accuracy to which SAGE calculates the out-of-focus beam profiles for NIF beams has not yet been experimentally determined, SAGE has accurately predicted the out-of-focus beam profiles for OMEGA beams. Figure 10 shows experimental data for the intensity of an OMEGA beam as a function of radius for best focus and two different defocus distances (5 mm and 10 mm). The theoretical calculations obtained from SAGE are plotted with the experimental data. The best focus was fit to a Gaussian of order n=7 [$I \propto \exp-(r/r_0)^n$ with r_0=380 μm], from which SAGE calculated the out-of-focus beam profiles. The accuracy to which SAGE calculates the out-of-focus profiles is excellent. It is reasonable to assume that SAGE will calculate the out-of-focus profiles of NIF beams to a similar degree of accuracy.

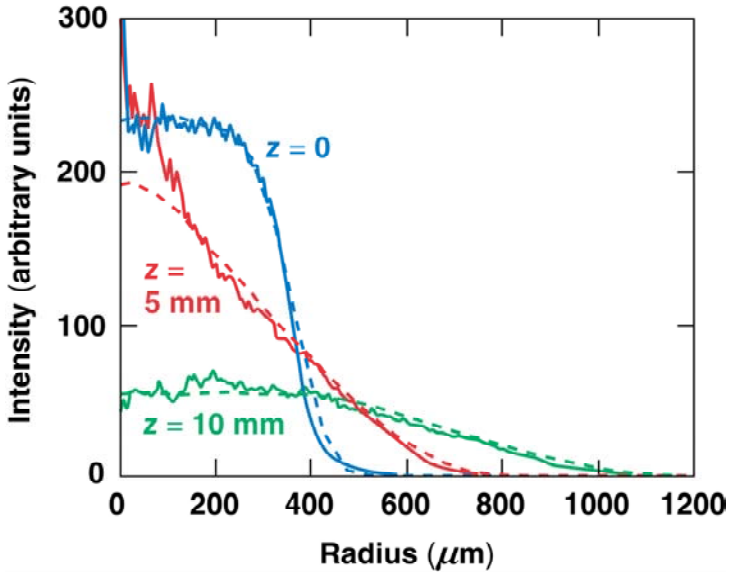

Figure 10. Graphs of intensity versus radius of an OMEGA beam at best focus (z=0) and for two defocus distances (z=5 mm and 10 mm). The solid lines correspond to experimental data and the dashed lines correspond to SAGE simulations.

4. Optimization Process and the Optimized Designs

The goal of the optimization process was to develop the design that would cause the shell to implode with the greatest degree of uniformity. Specifically, a design was sought that produced the lowest deviation of shell radius at a late time into the pulse (2.8 ns), just before the time of peak compression (see Figure 7). The optimization process involved running and

analyzing several hundred hydrodynamic simulations with different combinations of focusing and pointing parameters for each beam. The parameters that were varied included the shift, the defocusing distance, and the split-quad *y*-shift and *z*-shift for each ring of beams. The choice of run parameters came from analyzing the sensitivities to various parameters and from experimenting with the effects of varying different parameters. The main analysis was based upon plots of the center-of-mass radius versus angle from the vertical axis for different times (see Figure 11) with some guidance coming from raytrace plots. Plots of the center-of-mass radius show the areas of significant distortion. Figure 11(a) shows an example for an unoptimized design, which is to be compared with Figure 11(b) for the optimized design with phase plates. In Figure 11(a), the prominent bumps shown were typical of unoptimized designs. The level of uniformity decreases over time as slight distortions are magnified. In this example, the equator is particularly underdriven, resulting in a substantial bump there. The solution to this problem was a slightly tighter focus on the equator, to produce more equatorial drive. The other bumps are the results of beam profiles having relatively steep edges as in the top and bottom

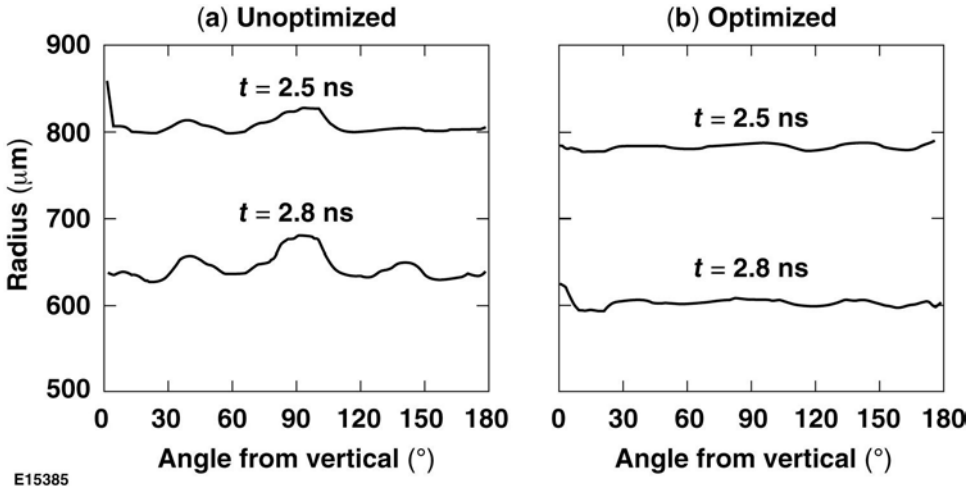

Figure 11. The center-of-mass radius plotted versus angle θ from the z-axis for unoptimized (a) and optimized (b) runs for the design with phase plates. These plots show which areas of the shell are receiving either too much drive or too little drive. In going from (a) to (b), the drive at the equator needed to be strengthened and the edges of rings three and four needed have a smoother overlap.

portions of Figure 5(d). When the edges of beams are steep, it is difficult to obtain equal amounts of drive at angles where the beams overlap. The solution to this was to increase the split-quad Δz shift on rings three and four slightly. Also, the simulation code sometimes produced some numerical noise such as the false peaks at $\theta=0°$ at 2.5 ns in Figure 11(a) and at 2.8 ns in Figure 11(b), but these were easy to identify and did not affect the overall optimization process. Overall the simulations showed consistent behavior as laser parameters were varied.

The final set of parameters for the design with phase plates are shown in Table 1; the parameters for the design without phase plates are in Table 2. These tables contain all the specifications needed to implement these designs on the NIF. Parameters of particular interest are the defocus distances and the split-quad shifts. As is evident, the defocus distance varies for the four rings, with the smallest defocus distance on ring four. This is to provide the extra drive needed at the equator by increasing the intensity of those beams. In the design with phase plates, split quads are used on rings three and four. For ring four, this smoothes out the steeper drop-off of intensity that would otherwise be present from the smaller defocus [compare Figures 5(d) and 6(d)]. The parameters for the design without phase plates are very similar, with the exception of the split quads. For this design, rings two, three, and four all require split quads. Without phase plates to spread the beam energy, the intensity drops off very quickly at the edge of the beam. For the design without phase plates, the split quad shifts are significantly larger than for the previous design. This provides the needed shift to alter the steep drop-off in beam intensity to a more gradual rate of decrease of intensity. The more gradual rate of decrease makes it easier to overlap the individual beams to provide the most uniform irradiation of the target.

Table 1. Beam parameter specifications for the optimum design using indirect-drive phase plates.

	Angle	Pointing Shift	Defocus Distance	Phase Plate	Split Quad Z-Shift	Split Quad Y-Shift
Ring 1	23.5°	50 μm	3.0 cm	Inner	----	----
Ring 2	30.0°	159 μm	3.5 cm	Inner	----	----
Ring 3	44.5°	250 μm	3.5 cm	Outer	212 μm	141 μm
Ring 4	50.0°	494 μm	1.7 cm	Outer	247 μm	155 μm

Table 2. Beam parameter specifications for the optimum design without phase plates.

	Angle	Pointing Shift	Defocus Distance	Split Quad Z-Shift	Split Quad Y-Shift
Ring 1	23.5°	53 μm	3.0 cm	----	----
Ring 2	30.0°	165 μm	3.5 cm	283 μm	458 μm
Ring 3	44.5°	250 μm	3.5 cm	283 μm	458 μm
Ring 4	50.0°	494 μm	1.7 cm	283 μm	458 μm

Both of these designs produced excellent shell radius uniformity. The design using phase plates had a root-mean-square deviation of radius (ΔR_{rms}) of approximately 4 μm at 2.8 ns, when the shell has imploded to a radius of 600 μm, half of its initial radius. The design without phase plates performed nearly as well, giving a root-mean-square deviation of radius of approximately 6 μm at the same time. Uniformity of velocity is also necessary to produce good compression. These designs produce uniformity of velocity to approximately 2% (rms) for the phase plate design and 4% (rms) for the design without phase plates.

The sensitivity of the designs to pointing errors has been explored. Ring four is the ring most sensitive to pointing errors because of the tighter focusing. The sensitivity to mispointings of this ring is shown in Figure 12 for the two designs. These plots show the ΔR_{rms} of pointing error in the worst case scenario, where all of the ring 4 beams are mispointed in the same direction. The values on the x-axis are the pointing errors relative to the optimum shift for ring four (494 μm). Some short-scale structure resulting from numerical noise in the simulations is

apparent very close to the optimum pointings. However, the graphs clearly show only a slight reduction of uniformity for errors in the ±50 μm range. The NIF pointing specification is 50 μm and pointings accurate to within 30 μm have been demonstrated[11]. Therefore, the pointing on the NIF is more than adequate to produce good uniformity using these designs.

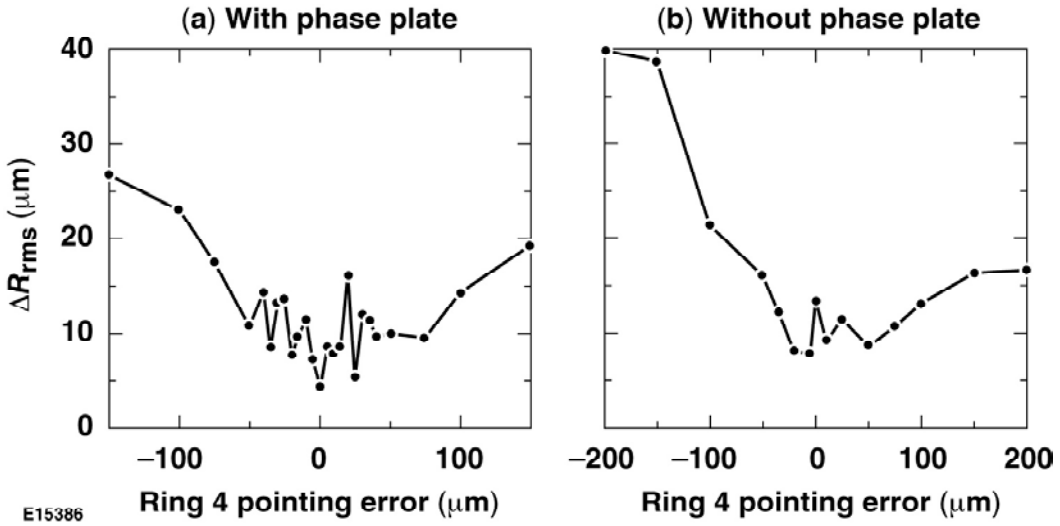

Figure 12. Sensitivity of the rms radius deviation at 2.8 ns to pointing errors of ring four from the optimum design in (a) the design with phase plates and (b) the design without phase plates.

5. Conclusion

Two experimental designs, including beam focus and pointing parameters, have been developed using hydrodynamic simulations to provide optimal implosion uniformity for directly-driven DT-gas-filled glass shells on the NIF. The development of these two designs makes it possible to carry out spherical implosions on the NIF as soon as all 192 beams are operational. In particular, high-neutron-yield implosions are possible on the NIF before the NIF is ready for ignition experiments. The availability of both a design using the NIF indirect-drive phase plates and a design using no phase plates allows for more flexibility according to what is available on the NIF at the time. These designs are necessary for initial experiments to test the NIF neutron diagnostic systems and will also enable direct-drive implosion experiments to be carried out much sooner than would otherwise be possible.

6. References

1. J. Nuckolls *et al.*, "Laser Compression of Matter to Super-High Densities: Thermonuclear (CTR) Applications," Nature **239**, 139 (1972).
2. J. D. Lindl, "Development of the Indirect-Drive Approach to Inertial Confinement Fusion and the Target Basis for Ignition and Gain," Phys. Plasmas **2**, 3933 (1995).
3. S. Skupsky *et al.*, "Polar Direct Drive on the National Ignition Facility," Phys. Plasmas **11**, 2763 (2004).
4. R. S. Craxton *et al.*, "Polar Direct Drive: Proof-of-Principle Experiments on OMEGA and Prospects for Ignition on the National Ignition Facility," Phys. Plasmas **12**, 056304 (2005).
5. J. A. Marozas *et al.*, "Polar-Direct-Drive Simulations and Experiments," Phys. Plasmas **13**, 056311 (2006).
6. R. S. Craxton and D. W. Jacob-Perkins, "The Saturn Target for Polar Direct Drive on the National Ignition Facility," Phys. Rev. Lett. **94**, 095002 (2005).
7. Y. Kato *et al.*, "Random Phasing of High-Power Lasers for Uniform Target Acceleration and Plasma Instability Suppression," Phys. Rev. Lett. **53**, 1057 (1984).
8. T. J. Kessler *et al.*, "Phase Conversion of Lasers with Low-Loss Distributed Phase Plates," in *Laser Coherence Control: Technology and Applications*, edited by H. T. Powell and T. J. Kessler (SPIE, Bellingham, WA, 1993), Vol. 1870, p. 95.
9. P. W. McKenty, Laboratory for Laser Energetics, private communication (2006).
10. R. S. Craxton and R. L. McCrory, "Hydrodynamics of Thermal Self-Focusing in Laser Plasmas," J. Appl. Physics. **56**, 108 (1984).
11. R. A. Zacharias *et al.*, "National Ignition Facility Alignment and Wavefront Control," in

Optical Engineering at the Lawrence Livermore National Laboratory II: The National Ignition Facility, edited by M. A. Lane and C. R. Wuest (SPIE, Bellingham, WA, 2004). Vol. 5341, p. 168.